Modeling and Experimental Verification of an Electromagnetic and Piezoelectric Hybrid Energy Harvester

Fan Yuanyuan[1,*], Sang Yingjun[2], Li Man[2], Wu Shangguang[2], Ding Zujun[2], Wang Yeqin[2] & Hao Yunrong[1]

[1]Faculty of Mathematics and Physics,
Huaiyin Institute of Technology, Huaian 223003, China
[2]Faculty of Automation, Huaiyin Institute of Technology, Huaian 223003, China
*E-mail: fyuanyuan123@163.com

Abstract. This paper describes mathematical models of an electromagnetic and piezoelectric hybrid energy harvesting system and provides an analysis of the relationship between the resonance frequency and the configuration parameters of the system. An electromagnetic and piezoelectric energy harvesting device was designed and the experimental results showed good agreement with the analytical results. The maximum load power of the hybrid energy harvesting system achieved 4.25 mW at a resonant frequency of 18 Hz when the acceleration was 0.7 g, which is an increase of 15% compared with the 3.62 mW achieved by a single electromagnetic technique.

Keywords: *ambient vibration; electromagnetic; energy conversion; energy harvesting; optimal load; piezoelectric energy conversion.*

1 Introduction

With the development of intelligent electric vehicles and miniature automobile sensors, the number of electric vehicle sensors will greatly increase. The energy supply to the very large number of tiny sensor nodes is an urgent problem to solve [1,2]. The sensor power can be provided by a battery, but this will make it difficult to maintain the electronic equipment and it will be harmful to the environment. In addition, in many cases it is inconvenient or even impossible to change the battery or charge it. Power wires could be used for sensor power supply as well, but in that case too many factors need to be considered when laying the power wires, such as the pressure of the wires, the length of the wires, the protection of the wires over sharp edges, and the lifetime of the wires near heat sources or moving parts. Furthermore, when the power supply wires of the sensors are in malfunction it is a waste of human resources to find the faulty wire among a large number of wires. Therefore, it is hoped that the sensor energy can be collected from vibration energy in the environment. This can extend the lifetime of low power consumption equipment and power the equipment separately instead of relying on batteries [3].

Received July 22nd, 2016, 1st Revision September 13th, 2016, 2nd Revision November 7th, 2016, Accepted for publication November 17th, 2016.
 ISSN: 2337-5779, DOI: 10.5614/j.eng.technol.sci.2016.48.5.8

Vibration is ubiquitous in a vehicle environment, so low-power vehicle sensors could be powered by recycling vibration energy. A number of researchers have reported the use of energy harvesting methods to improve the efficiency of vibration energy harvesting [4,5]. The advantages of vibration energy harvesting using piezoelectric materials are high availability, good performance, and high output voltage [6]. Electromagnetic energy harvesting is popular because of its convenient design, simple production and easy analysis [7].

A single power supply mode is not sufficient to meet the needs of electronic products. An electromagnetic and piezoelectric hybrid energy harvesting system (EPHEHS) could be used to solve the problem of low power supply [8-11]. In this study, a hybrid energy harvesting device combining piezoelectric technology and electromagnetic harvesting technology was designed and its power generation performance in the resonance condition was verified. The experimental results showed that the maximum load power of the device was 4.25 mW, which means an increase of 15% compared with the 3.62 mW achieved using a single electromagnetic technique when the resonance frequency was 18 Hz and the acceleration 0.7 g.

2 EPHEHS Structure and Mathematical Model

2.1 EPHEHS Structure and Principle

The structure of the vibration based hybrid energy harvesting device is shown in Figure 1(a). It is composed of a piezoelectric cantilever beam with a mass block at its end and a group of coils. The permanent-magnet mass block is used to excite the vibration and adjust the resonance frequency, while a varying magnetic field is provided for the coil placed underneath it. Electromagnetic energy conversion is realized through the relative motion between the permanent magnet and the coils, while the piezoelectric patches produce an electric charge under the effect of stress.

2.2 EPHEHS Mathematical Model

2.2.1 EPHEHS Vibration Model

Piezoelectric cantilevers are sensitive to ambient vibration. Thus forced vibration can be harvested. A single degree of freedom spring-mass-damping system can be used to describe the vibration model [1,2] of the cantilever beam under external vibration excitation, as shown in Figure 1(b). The model of the vibration system is

$$\ddot{z}(t)+2\xi\omega_{\mathrm{n}}\dot{z}(t)+\omega_{\mathrm{n}}{}^{2}z(t)=-\ddot{y}(t) \tag{1}$$

In Eq. (1),

$y(t)$: vibration displacement based on the external environment. $y(t) = Y\cos\omega t$;

$z(t)$: relative vibration displacement of the mass;

ξ : damping ratio, $\xi = c/2\sqrt{km}$, where C represents damping;

ω_n : the system's fundamental frequency vibration angular frequency, $\omega_n = \sqrt{K/m}$, K is the effective elastic coefficient of the system, m = Δm + 0.236 M [3], Δm is the mass of the mass block, M is the mass of the cantilever beam.

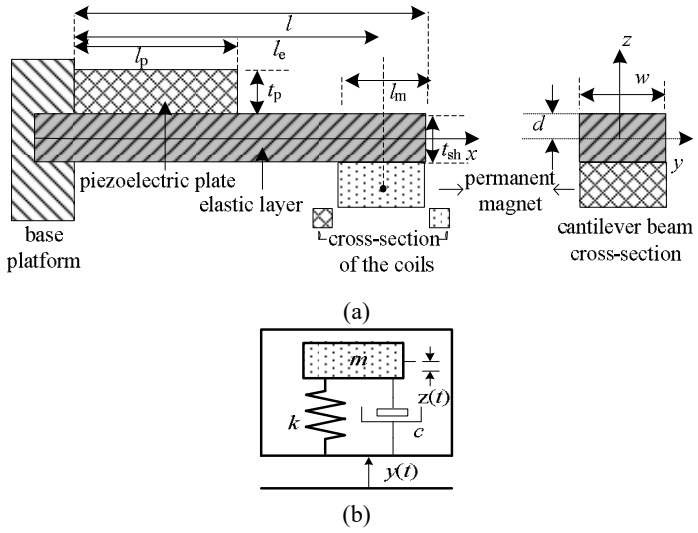

Figure 1 (a) Cantilever beam structure diagram, (b) spring-mass-damping system diagram.

The MATLAB software was used to obtain the complete solution, as follows in Eq. (2):

$$z(t) = A_0 e^{-\xi\omega_n t}\cos(\sqrt{\omega_n{}^2 - \xi^2\omega_n{}^2}\,t + \varphi_0) + A\cos(\omega t + \varphi) \tag{2}$$

The complete solution is the sum of the transient part and the steady state part, where the transient part is a damped vibration, which quickly decays to zero. Hence the solution can be expressed as follows, ignoring the transient part (See Eq. (3)).

$$z(t) = A\cos(\omega t + \varphi) = \frac{Y\left(\frac{\omega}{\omega_n}\right)^2}{\sqrt{(1-\left(\frac{\omega}{\omega_n}\right)^2)^2 + (2\xi\left(\frac{\omega}{\omega_n}\right))^2}}\cos(\omega t + \varphi) \tag{3}$$

According to the steady state solution, the average power consumption [1] of the system is calculated as follows in Eq. (4).

$$P = \frac{1}{T}\int_0^T czdz = \frac{m\xi Y^2\omega^3\left(\frac{\omega}{\omega_n}\right)^3}{(1-\left(\frac{\omega}{\omega_n}\right)^2)^2 + (2\xi\left(\frac{\omega}{\omega_n}\right))^2} \tag{4}$$

When $\omega = \omega_{n,}$ the output power of the vibration energy harvesting system is shown in Eq. (5).

$$P = \frac{m\omega_n^3 Y^2}{4\xi} \tag{5}$$

According to the cross-section conversion method [4] and the moment of inertia parallel axis theorem [5], when $x = 0 \sim l$p and $x = l$p $\sim l$e, the equivalent sectional moment of inertia is shown in Eq. (6).

$$\begin{cases} I_1 = \eta[\frac{wt_{sh}^3}{12} + wt_{sh}(\frac{t_{sh}}{2} - d)^2] + [\frac{wt_p^3}{12} + wt_p(\frac{t_p}{2} + d)^2] \\ I_2 = \frac{\eta wt_{sh}^3}{12} \end{cases} \tag{6}$$

In Eq. (6),

d: distance from the neutral axis to the lower surface of the piezoelectric layer, d = (ηtsh2 - tp2) /2(tp + ηtsh), tp and tsh are the thickness of the piezoelectric layer and the thickness of the elastic layer, respectively;

w: width of the cantilever beam;

η: $\eta = Y_{sh}/Y_p$, Y_{sh} *and* Y_p are the elastic modulus of the elastic layer and the piezoelectric layer, respectively.

From the theory of structural mechanics [4], the effective elastic coefficient of the cantilever beam is $K = \frac{3Y_p I_1 I_2}{(l_e^3 - (l_e - l_p)^3)I_2 + (l_e - l_p)^3 I_1}$

The fundamental frequency vibration angular frequency Equation of the system is shown in Eq. (7):

$$\omega_n = \sqrt{\frac{K}{m}} = \sqrt{\frac{3Y_p I_1 I_2}{[(l_e^3 - (l_e - l_p)^3)I_2 + (l_e - l_p)^3 I_1](\Delta m + 0.236M)}} \tag{7}$$

It is obvious that the resonance frequency is not only related to the material characteristics, the structure size of the cantilever beam and the frequency of the vibration environment, but also to the mass of the cantilever beam and the mass block. In low-frequency applications it is easier to adjust the resonance frequency by the mass of the mass block, because the cantilever beam is very thin and therefore its mass is small. The mass block is located at one end of the cantilever beam, which is relatively large and has a great impact on the resonance frequency.

2.2.2 EPHEHS Piezoelectric Model

From the piezoelectric equation [5] it is known that when the cantilever beam is under the action of inertia in the Z direction, the piezoelectric layer will generate tension and compression in the X direction and form a coupled electric field in the Z direction. For piezoelectric strain $\delta = -d_{31}E_3$, this can be equivalent to a concentrated force F_E at the end of the cantilever beam. Eq. (1) is transformed into the following Eq. (8) concerning the electric field force,

$$m\ddot{z}(t) + c\dot{z}(t) + kz(t) = -m\ddot{y}(t) - F_E(t) \tag{8}$$

The bending moment of cantilever beam X under the concentrated force in the Z direction is given by Eq. (9).

$$M_x = F\left(l_e - x\right) \tag{9}$$

According to the relationship between strain and bending moment: $\delta = Mz / Y_p I_1$, the strain of the piezoelectric layer is as shown in Eq. (10).

$$\delta = F(l_e - x)z / YI \tag{10}$$

The relationship between the piezoelectric strain and the equivalent electric field force is given by Eq. (11).

$$-d_{31}E_3 = F_E\left(l_e - x\right)z / Y_p I_1 \tag{11}$$

The piezoelectric ceramic material is a dielectric material, with metal electrode layers coated on the upper and the lower surface. Hence, the piezoelectric medium between both electrodes is equivalent to the capacitor. The equivalent capacitance is $C_P = S\varepsilon_{33}/t_p$, where ε_{33} is the dielectric constant of the piezoelectric material and S is the area of the piezoelectric layer. The electric field E_3 between the electrodes can be regarded as a uniform electric field, according to the electric field calculation equation between capacitor plates (see Eq.(12)),

$$E_3 = -\frac{U}{t_p} \tag{12}$$

U is the voltage between the electrodes of the piezoelectric ceramic. Hence, Eq. (11) is expressed as follows in Eq. (13),

$$\frac{d_{31}U}{t_p} = \frac{1}{l_p t_p}\iint \frac{F_E(l_e - x)z}{Y_p I_1}\mathrm{d}x\mathrm{d}z \tag{13}$$

The solution is $F_E = k_1 U$, $k_1 = 4\dfrac{d_{31}Y_p I_1}{(2l_b - l_p)(t_p + 2d)t_p}$。

When F_E is substituted into Eq. (8), z is obtained as follows in Eq. (14).

$$z = \frac{\omega^2 y - k_1 U/m}{-\omega^2 + j2\xi\omega\omega_n + \omega_n^2} \tag{14}$$

For the electromechanical coupling process of piezoelectric ceramics and according to the heat balance principle, the total energy of the piezoelectric layer is expressed as the internal energy [6] of the system generated by the infinitesimal unit, as follows

$$W = 2\int_{V_p}(\frac{1}{2}S^2 E_p - d_{31}E_p S\frac{U}{t_p} + \frac{1}{2}\varepsilon_{33}(\frac{U}{t_p})^2)\mathrm{d}V \tag{15}$$

Substituting Eq. (10) into the Eq. (15), only retaining the items relative to U, the electric field energy of the piezoelectric layer is

$$W_E = 2(-k_2 FU + \frac{1}{2}\frac{\varepsilon_{33}wl_p}{t_p}U^2) \tag{16}$$

In the Eq., $k_2 = \dfrac{d_{31}wl_p(2l_b - l_p)(t_p + 2d)}{4I_1}$.

Differentiating to voltage U in Eq. (16), the amount of charge on the piezoelectric layer is as shown in Eq. (17).

$$q=\frac{1}{2}\frac{\mathrm{d}W_{\mathrm{E}}}{\mathrm{d}U}=-k_2F+\frac{U\varepsilon_{33}wl_{\mathrm{p}}}{t_{\mathrm{p}}} \tag{17}$$

The equivalent capacitance of piezoelectric $C_{\mathrm{P}} = wl_{\mathrm{p}}\varepsilon_{33}/t_{\mathrm{p}}$. The differential calculation is done to the charge q and the current expression is as follows,

$$i=-\frac{\mathrm{d}q}{\mathrm{d}t}=k_2\frac{\mathrm{d}F}{\mathrm{d}t}-C_{\mathrm{p}}\frac{\mathrm{d}U}{\mathrm{d}t} \tag{18}$$

Substituting $F = |F|\mathrm{e}^{\mathrm{j}\omega t}$,$U = |U|\mathrm{e}^{\mathrm{j}\omega t}$ in Eq.(18), the following equation is obtained

$$\frac{Fk_2}{C_{\mathrm{P}}}=U+\frac{i}{\mathrm{j}\omega C_{\mathrm{P}}} \tag{19}$$

The external force of the cantilever beam is equivalent to

$$F=Kz \tag{20}$$

Bringing Eqs. (14) and (20) into Eq. (19) and arranging it gives Eq. (21).

$$\left(\frac{\frac{Kk_2}{C_{\mathrm{P}}}\omega^2 y}{-\omega^2+\mathrm{j}2\xi\omega\omega_{\mathrm{n}}+\omega_{\mathrm{n}}{}^2(1+k_{\mathrm{p}})}\right)= U+\frac{i\left(-\omega^2+\mathrm{j}2\xi\omega\omega_{\mathrm{n}}+\omega_{\mathrm{n}}{}^2\right)}{\mathrm{j}\omega C_{\mathrm{P}}\left(-\omega^2+\mathrm{j}2\xi\omega\omega_{\mathrm{n}}+\omega_{\mathrm{n}}{}^2(1+k_{\mathrm{p}})\right)} \tag{21}$$

In the Eq., $k_2=\frac{d_{31}wl_{\mathrm{p}}(2l_{\mathrm{b}}-l_{\mathrm{p}})(t_{\mathrm{p}}+2d)}{4I_1}$, $k_{\mathrm{p}}=\frac{k_1k_2}{C_{\mathrm{P}}}=\frac{d_{31}{}^2Y_{\mathrm{p}}}{\varepsilon_{33}}$, when $i = 0$ the relationship between the open circuit voltage and the vibration angular frequency can be expressed as in Eq. (22).

$$V_{\mathrm{o}}=\left(\frac{\frac{Kk_2}{C_{\mathrm{P}}}A_{in}}{-\omega^2+\mathrm{j}2\xi\omega\omega_{\mathrm{n}}+\omega_{\mathrm{n}}{}^2(1+k_{\mathrm{p}})}\right) \tag{22}$$

The acceleration of the external excitation vibration $A_{in} = \omega^2 y$.

When external load R is connected, the piezoelectric layer capacitance is assumed to be Xc. Then the average output power [11] can be expressed as follows in Eq. (23).

$$P_p = \frac{1}{T}\int_0^T \frac{RV_o^{\,2}}{(Xc+R)^2}dt = \frac{1}{2}\frac{RV_o^{\,2}}{(Xc+R)^2} \tag{23}$$

2.2.3 EPHEHS Electromagnetic Model

By deriving from vibration model Eq. (1), the EPHEHS electromagnetic model is obtained as follows in Eq. (24):

$$z(t)=Z\sin(\omega t-\varphi)=Y\cdot\omega^2\cdot\sin(\omega t-\varphi)/\left\{(\omega_n^2-\omega^2)^2+(c\omega/m)^2\right\}^{1/2} \tag{24}$$

The electric potential is equal to the change rate of magnetic flux to time. When changing magnetic field S is an area that passes through a closed-loop coil, the induced electromotive force can be expressed as

$$\varepsilon = -d\phi / dt = -\int_S (d\vec{B}/dt)\cdot dS - \oint_C (\vec{B}\cdot z)\cdot dl \tag{25}$$

The magnetic flux density, B, around the magnet changes with the change of the spatial position, which is shown in the Figure 2. If K is assumed to be a coefficient relative to the position of the magnet, the coil and magnetic flux density B, then K is less than or equal to 1 and will decrease with the increase of the distance between the magnet and the coil. The relative motion of the permanent magnet and the coil is governed by the sine rule under the action of the sine excitation, so magnetic flux density B_1 and B_2 can be expressed as

$$\begin{cases} B_1 = K_1\cdot B(\omega) = K_1\cdot[B_M\cdot\cos(\omega t-\varphi)\vec{z} + B_M\cdot\cos(\omega t-\varphi)\vec{x}] \\ B_2 = K_2\cdot B(\omega) = K_2\cdot[B_M\cdot\cos(\omega t-\varphi)\vec{z} + B_M\cdot\cos(\omega t-\varphi)\vec{x}] \end{cases} \tag{26}$$

BM is the maximum value of the permanent magnet flux density. Substituting Eq. (26) into Eq. (25), the electromotive force can be calculated as follows in Eq. (27).

$$\begin{aligned} \varepsilon &= -\int_0^{2\pi}(d\vec{B}/dt)\cdot\frac{1}{2}\cdot r^2\cdot d\delta - \int_0^{\pi}(\vec{B}\cdot z)\cdot r\cdot d\delta + \int_{\pi}^{2\pi}(\vec{B}\cdot z)\cdot r\cdot d\delta \\ &= \pi r^2 K B_M \omega\sin(\omega t-\varphi) \\ &+ \pi r K_1 B_M \omega^3 Y\sin(\omega t-\varphi)\sin(\omega t-\varphi)/\left\{(\omega_n^{\,2}-\omega^2)^2+(c\omega/m)^2\right\}^{1/2} \\ &- \pi r K_2 B_M \omega^3 Y\sin(\omega t-\varphi)\sin(\omega t-\varphi)/\left\{(\omega_n^{\,2}-\omega^2)^2+(c\omega/m)^2\right\}^{1/2} \end{aligned} \tag{27}$$

In the Eq., r is the radius of the coil; δ is the circumferential angle; K_1、K_2 are the magnetic flux density coefficient of the vertical component of the magnetic field in different spatial positions, which can be estimated by measuring the ratio of the magnetic force at its position to the maximum magnetic force. If the space position of the coil and the intermediate shaft of the permanent magnet magnetic field is symmetrical, then $K_1 = K_2$. In this case, taking into account the number of turns of coil N, the electric potential of the coil is estimated to be (see Eq. (28)):

$$\varepsilon = \pi r^2 NKB_M \omega \sin(\omega t - \varphi) \tag{28}$$

When coil resistance R_s and output resistance R_o are given, the average power of the electromagnetic output is as shown in Eq. (29).

$$P_e = \frac{1}{T}\int_0^T \frac{R_o \varepsilon^2}{R_s + R_o} dt = \frac{1}{2}\frac{R_o(\pi r^2 NKB_M \omega)^2}{R_s + R_o} \tag{29}$$

The total output power of the hybrid vibration power generation system is $P_o = P_p + P_e$. It is obvious that the size of the output power is relative to the resonant frequency of the piezoelectric cantilever beam, the size of the piezoelectric plate, the characteristics of the material, the parameters of the external load, the parameters of the coil winding, the magnetic induction intensity and so on.

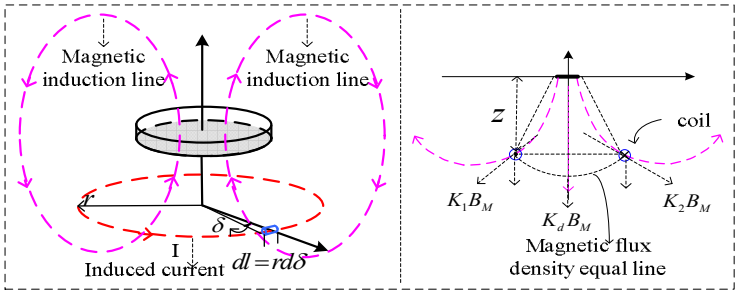

Figure 2 Magnetic induction curve distribution.

2.2.4 Analysis of System Damping Ratio

The damping of the hybrid vibration power generation system consists of three main parts, i.e. mechanical damping, piezoelectric damping and electromagnetic damping. From Eq. (5), the damping ratio of the system is in Eq. (30).

$$\xi = m\omega_n^3 Y^2 / 4P \tag{30}$$

By combining the resonance frequency Eq. with the average power Eq. it is clear that the system damping ratio is mainly related to the resonance frequency

of the system, the frequency of the vibration environment, the geometry size, the mass of the mass block and the external load, in which the electromagnetic damping ratio is also related to the magnetic field strength and the coil parameters.

The amplitude of the cantilever beam will be reduced as the external load increases system damping. For the piezoelectric unit, due to the influence of the secondary piezoelectric effect, with the increase of the external load, the resonance frequency will increase slightly [11].

3 EPHEHS Simulation Analysis

Numerical simulation of the EPHEHS model was carried out using the MATLAB software. The relationships between the resonant frequency of the piezoelectric cantilever beam and the length of the cantilever beam, the width of the cantilever beam, the length of the mass, the height of the mass and the structure parameters of the piezoelectric ceramic chip are shown in Figures 3 to 5.

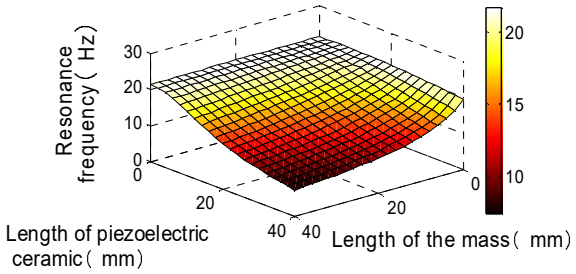

Figure 3 Relationship between resonance frequency, length of piezoelectric ceramic and length of the mass.

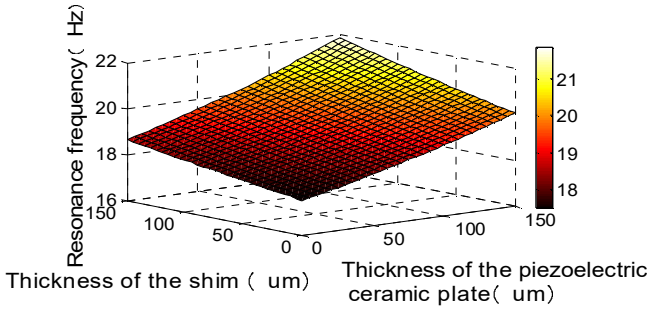

Figure 4 Relationship between resonance frequency, thickness of the piezoelectric ceramic plate and thickness of the shim.

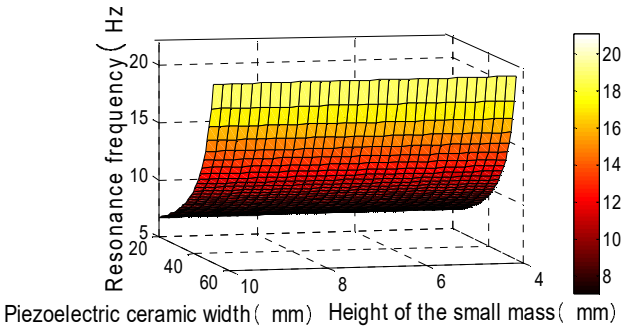

Figure 5 Relationship between resonance frequency, piezoelectric ceramic width and height of the small mass.

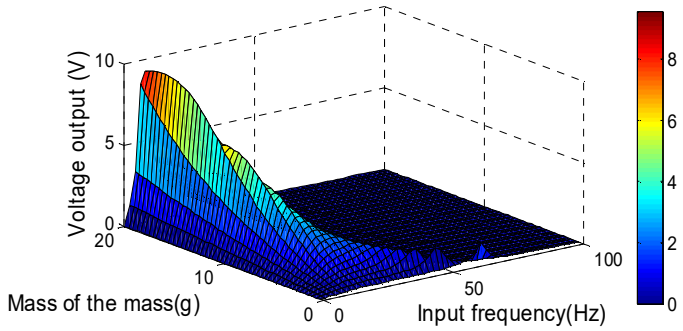

Figure 6 Output voltage – mass of the mass-input frequency curve.

In Figure 3 it can be seen that the resonance frequency decreases with the increase of the length of the piezoelectric ceramic sheet when the length of the mass of the cantilever beam is determined. The resonance frequency decreases with the increase of the length of the mass block in a certain length of the piezoelectric ceramic sheet. In Figure 4 it can be seen that the resonant frequency of the piezoelectric cantilever increases with the increase of the thickness of the piezoelectric ceramic sheet and the thickness of the metal gasket. In Figure 5 it can be seen shown that the resonant frequency of the piezoelectric cantilever beam increases with the increase of the width of the cantilever beam when the height of the small mass is constant. Meanwhile, the resonance frequency of the piezoelectric cantilever beam does not change with

the change of the height of the small mass when the width of the cantilever beam is determined.

Through the simulation, the relationship between the output voltage, the mass of the mass block and the input frequency is obtained, as shown in Figure 6. It can be seen that the output voltage of the system increases with the increase of the mass of the mass block; the change in color reflects the change of the output voltage at a certain vibration frequency. The output voltage of the system at the resonance frequency is higher than that at other frequencies. Hence, when the mass of the mass block is certain, the numerical value of the resonant frequency can be determined. It can be seen that the resonant frequency of the cantilever beam decreases with the increase of the mass of the mass block and that its influence on the resonance frequency is gradually weakened with the increase of the mass of the mass block.

The simulation analysis shows that the resonance frequency of the harvesting device is associated with the structure parameters of the cantilever. The resonance frequency of the system can be adjusted by changing the length, width and thickness of the piezoelectric plate and the substrate. According the numerical simulation of the EPHEHS model, a model was designed based on the COMSOL Multiphysics software. A structure diagram and mesh differential diagram of the system are shown in Figures 7 and 8.

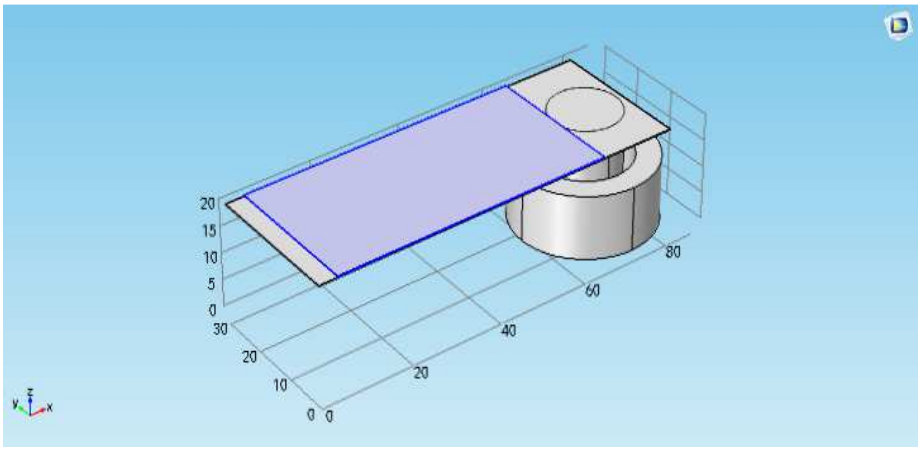

Figure 7 System structure diagram.

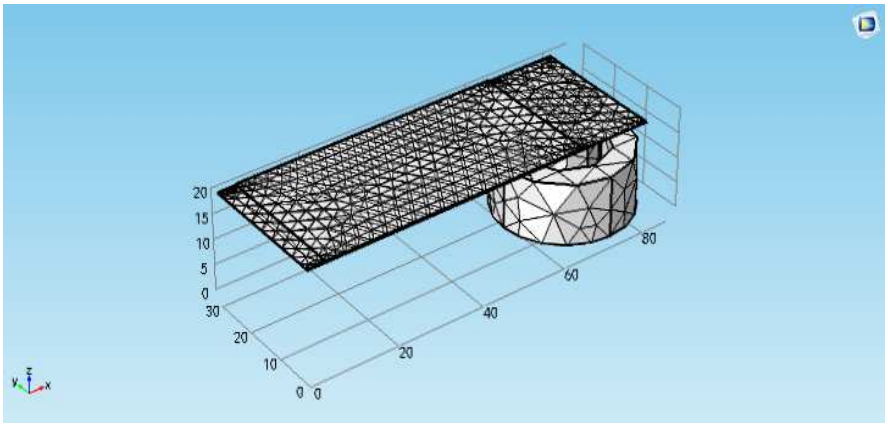

Figure 8 System mesh differential diagram.

The resonance frequency of the system was designed to be 18 Hz and the main parameters of the piezoelectric cantilever can be obtained by the sweep frequency when the material properties are added in the COMSOL Multiphysics software. The appropriate parameters for the piezoelectric cantilever are shown in Table 1.

Table 1 Feature parameters of hybrid harvester.

Parameter	Value	Parameter	Value
Length of the cantilever (mm)	80	Width of the cantilever beam (mm)	30
Length of the piezoelectric plate (mm)	60	Width of the piezoelectric plate (mm)	30
Material of the mass block	NdFeB	Density of the mass block (kg/m^3)	7500
Diameter of the mass block (mm)	7.5	Height of the mass block (mm)	20
Thickness of the gasket (mm)	0.2	Thickness of the piezoelectric layer (mm)	0.2
Wire diameter of the coil (mm)	0.10	The resistance of the coil (Ω)	1486
Inner diameter of the coil (mm)	18	The outer diameter of the coil (mm)	38
Young's modulus of the cantilever (GPa)	110	Young's modulus of the mass block (GPa)	65
Poisson ratio of the cantilever	0.35	Poisson ratio of the mass block	0.3
Piezoelectric dielectric constant	3 800 ε_0	Vacuum dielectric constant ε_0	8.854
Piezoelectric coefficient	320	Electromechanical coupling coefficient	0.5

4 EPHEHS Performance Test and Analysis

4.1 EPHEHS Experiment

The equipment used in the experiment consisted mainly of a signal generator, a power amplifier, a vibration exciter, an oscilloscope and a digital multimeter. The control signal is generated by the signal generator, which is amplified by the power amplifier. Then the vibration exciter starts working and applies the forced vibration to the cantilever beam. The oscilloscope is used to measure the generated AC voltage signal directly and the digital multimeter measures the load voltage after the bridge rectifier. By adjusting the frequency and amplitude of the control signal, the vibration frequency and the output voltage of the collecting device can be controlled. In the experiment, the vibration frequency was 18 Hz and the vibration acceleration was 0.7 g.

Figure 9(a) shows the composition of the experimental system. Figure 9(b) shows a photo taken during the field experiment; the oscilloscope shows the waveforms of the open circuit output voltage of the piezoelectric and electromagnetic mechanism.

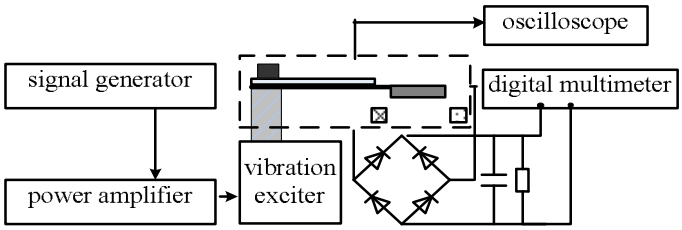

(a)

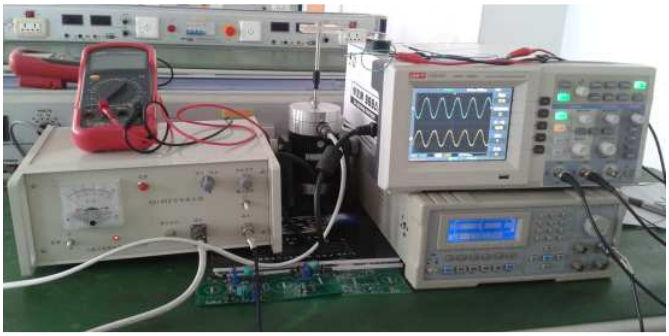

(b)

Figure 9 (a) Composition of the experimental system, (b) photo of the experimental system.

4.2 EPHEHS Experimental Results Analysis

The optimal load resistance of the hybrid energy harvesting device was determined by the parameters of the internal equivalent circuit and the switching circuit, whose value was determined as 1.5 kΩ using the PSPICE circuit simulation and the experimental method. The simulation results and the measured values of the load voltage and load power at the resonant frequency are shown in Figures. 10(a) and 10(b). From the figures it can be seen that the load power first increased and then reached peak value at the optimal load resistance. When the load resistance was greater than 1.5 kΩ, there was an obvious decrease in the load power. However, the load voltage increased with increasing load resistance. At the optimal load resistance, the load voltage calculated by the numerical simulation was 3.9 V, while the measured value was 3.57 V.

Figure 10(c) shows the optimal load powers of the hybrid and the single energy harvesting technique at the optimal load resistance from the experiment. Compared with the 3.62 mW load power obtained from the single type electromagnetic technique at the resonant frequency, the maximum load power of 4.25 mW was increased by 15%. The optimal load power was low under the single piezoelectric mode with the stable value at 0.9 mW. It is worth mentioning that the charging time of the piezoelectric mode was about 10 hours to achieve stable output. The charging time of the single electromagnetic mode was about 0.75 hours to achieve stable output. In addition, when the hybrid energy harvesting device was connected to the external load, there was a slight decrease in the amplitude of the vibration due to the existence of electromagnetic damping of the coil, which leads to a decrease in the amplitude of the voltage, thus the power also has a certain reduction. Therefore, the optimal load power of the hybrid energy harvesting device was slightly lower than the sum of the single electromagnetic and the piezoelectric operating modes.

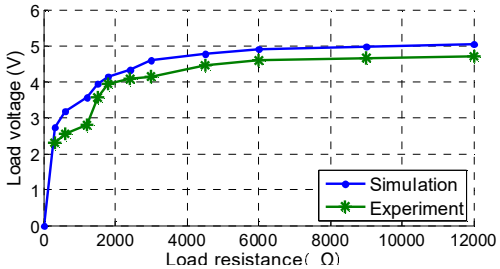

（a）Load voltage–load resistance diagram.

Figure 10 Comparison of simulation and experimental results.

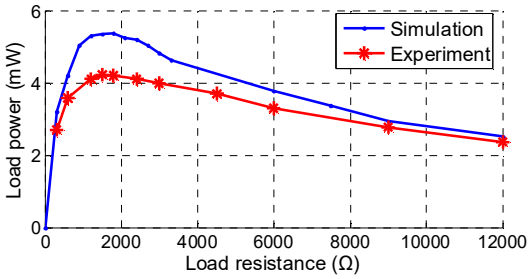

(b) Load power–load resistance diagram.

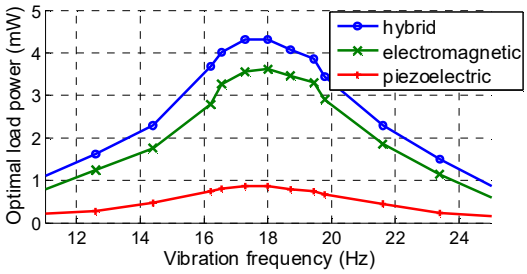

(c) Optimal load power–vibration frequency plot.

Figure 10 ***Continued.*** Comparison of simulation and experimental results.

5 Conclusions

Electromagnetic and piezoelectric hybrid energy harvesting systems can improve energy density effectively. In this paper, the mathematical model of such a system was given, the simulation analysis was presented and the performance of the proposed hybrid energy harvesting device was verified experimentally. At a resonant frequency of 18 Hz, the acceleration was 0.7 g, the maximum load power of the hybrid energy harvesting device was 4.25 mW, and the maximum load power was increased by 15% compared to the single electromagnetic technique.

Acknowledgments

This work was supported in part by National Natural Science Foundation of China (grant no. 51307070, 51505173), Six Talent Peaks Project of Jiangsu Province (2016-XNYQC-001), Jiangsu Provincial Education Department Project (No. 14KJB510006), and Huaian Science and Technology Plan Project (HAG2014037).

References

[1] Williams, C.B. & Yates, R.B., *Analysis of a Micro Electric Generator for Micro Systems,* Sensors and Actuators: Physical, **52**(1-3), pp. 8-11, 1996.

[2] Ng, T.H. & Liao, W.H., *Feasibility Study of a Self-Powered Piezoelectric Sensor,* Smart Structures and Materials 2004: Smart Electronics, MEMS, BioMEMS, and Nanotechnology. San Diego, United States, Proceedings of SPIE 5389, pp. 377-388, 2004.

[3] Hibbeler, R.C., *Mechanics of Materials,* United States, Pearson Prentice Hall publisher, 2005.

[4] Beer, F.P., Johnston, E.R. & Eisenberg, E.R., *Vector Mechanics for Engineers,* United States, McGraw-Hill publisher, 2004.

[5] Yu, H., Zhou, J., Deng, L. & Wen, Z., *A Vibration-Based MEMS Piezoelectric Energy Harvester and Power Conditioning Circuit*, Sensors (Switzerland), **14**(2), pp. 3323-3341, 2014.

[6] Kan, J., Tang, K., Wang, S., Yang, Z., Jia, J. & Zeng, P., *Modeling and Simulation of Piezoelectric Cantilever Generators*, Optics and Precision Engineering, **16**(1), pp. 71-75, 2008.

[7] Zhao, X. & Wen, Z., *Resonant Frequency adjusting of Vibration Energy Harvester Based on Piezoelectric Materials*, Piezoelectrics & Acoustooptics, **35**(2), pp. 241-244, 2013.

[8] Yang, B., Lee, C., Kee, W.L. & Lim, S.P., *Hybrid Energy Harvester Based on Piezoelectric and Electromagnetic Mechanisms*, J. Micro-Nanolithogr. MEMS MOEMS, **9**(2), pp. 023002(1)-023002(10), 2010.

[9] Siddique, A.M., Mahmud, S. & Van Heyst, B., *A Comprehensive Review on Vibration Based Micro Power Generators using Electromagnetic and Piezoelectric Transducer Mechanisms*, Energy Conversion and Management, **106**, pp. 728-747, 2015.

[10] Salim, M., Aljibori, H.S.S. & Salim, D., *A Review of Vibration-Based MEMS Hybrid Energy Harvesters,* Journal of Mechanical Science and Technology, **29**(11), pp. 5021-5034, 2015.

[11] Liu, C.X., *A Hybrid Piezoelectric-electromagnetic Power Generation Technology and the Experimental Study*. Harbin, Harbin Institute of Technology, 2012.